MICROBIALLY DEPOSITED MANGANESE AND IRON OXIDES ON PASSIVE METALS -

THEIR CHEMISTRY, DISTRIBUTION, AND CONSEQUENCES FOR MATERIAL

PERFORMANCE

X. Shi
Center for Biofilm Engineering, Montana State University
Bozeman, MT 59717-3980, USA

R. Avci
Image and Chemical Analysis Laboratory
Department of Physics, Montana State University
Bozeman, MT 59717-0350, USA

Z. Lewandowski
Center for Biofilm Engineering, Montana State University
Bozeman, MT 59717-3980, USA and
Department of Civil Engineering, Montana State University
Bozeman, MT 59717-3900, USA

ABSTRACT

316L stainless steel and Ti-6Al-4V corrosion coupons exposed to fresh river water ennobled the open circuit potential (OCP) to values of +365 mV_{SCE} and +400 mV_{SCE}, respectively. ToF-SIMS spectra indicated that the biominerals on the metal surfaces are a mixture of Fe_2O_3, Mn_3O_4, and $MnOOH$ on fully ennobled coupons, while a mixture of Fe_3O_4, Fe_2O_3, Mn_3O_4, and Mn_2O_3 on partially ennobled coupons. Biomineralized manganese and iron oxides on the 316L stainless steel surfaces, regardless of the oxidation states, endanger the material integrity in a similar manner, as evidenced by the elevated OCP and increased cathodic current density upon mild polarization.

Keywords: biomineralization, microbially influenced corrosion (MIC), ToF-SIMS (time-of-flight secondary ion mass spectroscopy), ennoblement, manganese oxidizing bacteria (MOB), 316L stainless steel

INTRODUCTION

Microbially deposited minerals on water-immersed metal surfaces play an important role in microbially influenced corrosion (MIC) [1-7]. Therefore, identifying the active biomineralization processes that occur on the metal surfaces in natural waters provides a convenient point of departure to study MIC, and to study general metal–microbe interactions. For example, the corrosion mechanisms modified by the presence of sulfate-reducing bacteria (SRB) and manganese-oxidizing bacteria (MOB) [3] were revealed by demonstrating that the nature of MIC in both cases depended on the chemical composition of inorganic materials precipitated at the metal surface: iron sulfides and manganese oxides. These minerals, being electrochemically active, and remaining in electrical contact with the surface, modified electrochemical processes naturally occurring at the metal-solution interface and accelerated corrosion. Practical effects of biomineralization on corrosion may be exemplified by the failure of 304L piping at the Robinson Nuclear Power Station after 13-year exposure to untreated water containing only 3 ppm chloride and 6 ppm sulfate [8]. The inner surfaces of the pipes were covered with 1/4-inch thick microbial deposits containing 37wt.% manganese, and the mechanism of accelerated corrosion was attributed to MOB activity.

Recent studies have demonstrated that biomineralization of manganese is responsible for *ennoblement* of stainless steels, one of the most puzzling phenomena associated with MIC. Ennoblement, a subject of continual controversy since its discovery [9-16], features microbial colonization of passive metals followed by an increase in the open circuit potential (OCP), reaching final values between $+200$ mV$_{SCE}$ [11] and $+450$ mV$_{SCE}$ [9,13], accompanied by an increase in cathodic current density upon mild polarization of the ennobled samples[16]. In some instances and for some materials, the ennobled OCP approaches the critical pitting potential of the passive metal, which increases the risk of localized corrosion. As an example, turbine runner blades in a hydroelectric power plant [17,18] were severely damaged. The mechanism of the material failure was not immediately obvious because chloride concentration in the water (20-170 mg/L) was not high enough to cause pitting of the turbine material (CrNi134). SEM/EDAX and x-ray diffraction analyses of deposits removed from the corroded blades showed presence of manganese-containing minerals (approximately 25 wt.% MnOOH and 8 wt.% MnO$_2$), and the deposits had high OCP ($+570$ mV$_{SHE}$), characteristic of ennoblement. It was concluded that the high OCP was due to the reduction of manganese dioxide to divalent manganese.

In the authors' laboratory, Dickinson et al. [19, 20] studied effects of manganese oxidizing bacteria on stainless steels and demonstrated that 3% to 5% surface coverage by biofouling deposits was enough to ennoble the potential of 316L stainless steel. Chemical examination of the deposits [16] showed the presence of Fe(III) and Mn(IV), while epifluorescence microscopy revealed the presence of manganese- and iron-oxidizing bacteria. Based on these observations and other studies conducted in our laboratory [21-24] we have suggested that the MOB involvement in corrosion of stainless steels is based on the following mechanism: the divalent manganese (Mn^{2+}) ions are microbially oxidized to manganese oxyhydroxide, MnOOH, which is deposited on the metal surface, then the solid MnOOH is further oxidized to manganese dioxide, MnO$_2$. Both reactions contribute to the increase in the OCP because the deposited oxides, MnOOH and MnO$_2$, are in electrical contact with the surface and their dissolution potential is determined by the equilibrium of deposited minerals with the dissolved divalent manganese. The oxides, deposited on the surface, are reduced to the divalent manganese by electrons generated at anodic sites. However, reducing the manganese oxides does not stop the ennoblement process, because the reduced products of this reaction, soluble divalent manganese ions, are reoxidized by the MOB attached to the metal surface. The described sequence of events, oxidation-reduction-oxidation of manganese, is a hypothetical mechanism which produces renewable cathodic reactants, manganese

oxyhydroxide and manganese dioxide, and their presence on the metal surface endangers material integrity.

We have partially verified this hypothetical mechanism by defining surface chemistry of the microbial deposits and demonstrating, under well-defined laboratory conditions, that 316L stainless steel exposed to manganese-oxidizing bacteria, *Leptothrix discophora* SP-6, in a mineral-salt-pyruvate-vitamin medium containing Mn^{2+} ennobled to the same extent as the coupons exposed to natural waters. The coupons ennobled under well-defined laboratory conditions exhibited electrochemical characteristics, in terms of OCP and potentiodynamic polarization plots, almost identical to the corrosion coupons ennobled in natural waters [23]. However, this was just a laboratory study, and the results had to be corroborated by field studies before concluding that such a mechanism is indeed active in natural waters. The difficulties with conducting field studies to verify the hypothesis are in examining the chemistry of the microbial deposits, which are more complex than the deposits from laboratory studies. Before drawing definite conclusions suitable analytical techniques had to be used to demonstrate the sequence of chemical transitions on metal coupons exposed to natural waters. This paper describes our efforts toward adapting Time of Flight Secondary Ion Mass Spectroscopy (ToF-SIMS) as a surface analytical technique suitable for analyzing the biomineralized deposits on stainless steels exposed to natural waters. We used this technique to test the hypothesis proposed in our laboratory studies.

The chemistry of microbial deposits on solid surfaces is difficult to define; different microorganisms seem to deposit different minerals, and the deposited minerals are not stable, but their chemistry change in time. For example, Mn oxides formed by spores of different *Bacillus* spp. and sheathed *Leptothrix* resemble vernadite, δ-MnO_2, whereas a microalga, *Chlamydomonas* deposits manganite ($\gamma MnOOH$) [25]. As time progresses the composition of the deposits changes. An amorphous Mn oxide deposited by a marine *Bacillus* sp. (SG-1) later recrystallized to hausmannite (Mn_3O_4) [25], and the octahedral hausmannite formed by the SG-1 spores aged to MnO_x (x=1.9) over a period of weeks [26]. It has been suggested [27] that the biomineralized manganese is a mixture of birnessite and pyrolusite (MnO_2), manganite (MnOOH), and other oxides, and that microbial deposits have typically highly disordered structure. The analysis of the microbial deposits on surfaces of field ennobled 316L SS coupons using X-ray photoelectron spectroscopy (XPS) [21, 22] revealed a mixture of different manganese minerals with the chemistry not clearly identified. The electrochemical analysis using Cyclic voltammetry [5] detected MnO_2 in the biomineralized manganese oxides formed on metal surfaces in natural waters, but failed to identify other phases.

Our laboratory experiments have dealt entirely with MOB and biomineralized manganese oxides. However, it is well known that biomineralized deposits in natural waters are usually manganese deposits mixed with iron deposits. Also, the biomineralized iron oxides as well as manganese oxides have been implicated in MIC: iron oxide formation could initiate under-deposit corrosion of susceptible metals [4]. In a failure case of 304L and 316L SS tanks and pipes [28] that were partially filled with well water containing about 200 ppm chloride, surface deposits contained manganese and iron and both iron oxidizing bacteria (IOB) and MOB were identified. Therefore, iron oxides have to be included in any MIC-relevant description of chemistry of biomineralized deposits on stainless steels in natural waters. Including iron oxides adds complexity to the already complicated problem, since the chemical composition of biomineralized iron deposits is at least as difficult to establish, as it is to define that of biomineralized manganese deposits. Oxide films formed on iron in air consist of magnetite and hematite (Fe_2O_3) [4]. Ferric oxyhydroxides, including of α–FeOOH (goethite) and γ–FeOOH (lepidocrocite), have also been identified in protective layers on carbon steel. The Raman spectra [7] of deposits obtained from 304L pipework that had failed by MIC in iron-rich potable water revealed the presence of a mixture of

α–FeOOH and γ–FeOOH. A simulation experiment indicated that FeOOH deposits can be transformed, first to Fe_2O_3 and then to Fe_3O_4. Another complicating factor in the analysis of MIC-associated biomineralized oxides is the possible chemical reactions between manganese oxides and iron oxides.

As the surface analytical technique to analyze the biomineralized deposits we have used ToF-SIMS, which offers high detection sensitivity and chemical imaging [29,30], can detect elements as well as chemical compounds, can differentiate among isotopes, and allows mass imaging of deposits with submicron spatial resolution [31]. Using computerized data collection and retrospective analysis, the two-dimensional imaging of spatial distribution of chemical composition is possible. Due to its chemical imaging capabilities, SIMS has been applied to study the chemistry and distribution of oxides. For example, the distribution of ^{18}O, Fe and Cr in an oxide scale grown on 9% Cr/Fe steel was obtained and found informative in understanding the corrosion mechanisms [32], and depth profiling of oxide layers was done to investigate a corroded zircaloy fuel rod cladding specimen [31]. In another case, the ratios MO_2^- /MO^- and MO_3^-/MO^- for transition metal oxides of the type M_xO_y were measured to identify their oxidation state. The data for iron oxide were then compared to those for the oxide found on a steel sample with an oxide film 4 nm thick, and the best match was to Fe_2O_3 [29]. In the authors' laboratory, a technique based on ToF-SIMS [24] has been developed to identify the biominerals on 316L SS and Ti-6Al-4V corrosion coupons ennobled by the biofilm of MOB, *Leptothrix discophora* SP-6. The experimental results were statistically reproducible and the technique demonstrated reliable performance for surface sensitive analysis. We found that the microbial deposits on ennobled coupons consist of manganese oxyhydroxide (MnOOH) and manganese dioxide (MnO_2).

We have failed to verify the mechanism of ennoblement by determining the chemical composition of microbial deposits on stainless steel coupons because elements in the base metal, iron and manganese, have interfered with the secondary ion peaks in the SIMS spectra of microbial deposits on the ennobled coupons. For example, MnH^+ generated by microbial deposits and the metal substratum could not be differentiated from Fe^+ generated by the metal substratum. The extent of this interference was unknown because we did not have an independent standard to assess these contributions. To eliminate the effects of alloying elements we used two types of coupons, 316L stainless steel and low-iron titanium alloy (Ti-6Al-4V), and exposed them to the same environments. Assuming that the chemical nature of the deposits was the same on both coupons, any differences in the SIMS spectra would have to reflect the contribution of iron in the stainless steel coupons. Implementing this strategy, the SIMS spectra of the deposits on the Ti-6Al-4V coupons were used to verify the conclusions obtained from analyzing the deposits on 316L stainless steel coupons. The goal of this work was to analyze the chemical composition of biomineralized manganese and iron deposited on passive metals in natural waters. We placed a set of 316L stainless steel and Ti-6Al-4V corrosion coupons in a fresh water creek in Bozeman, MT, for ennoblement. Then, the composition of the surface deposits was determined by comparing the SIMS spectra of the deposits with spectra of manganese standards, MnO_2, MnOOH, Mn_3O_4, MnO, Mn_2O_3 and $MnCO_3$, and iron standards, FeO, Fe_2O_3, Fe_3O_4, and FeOOH. As a result, we have defined the chemistry of deposits and spatial distribution of microbially deposited minerals on the metal samples. In addition, we applied electrochemical techniques to evaluate the consequences of depositing biomineralized manganese and iron oxides on the OCP and current density generated during potentiodynamic polarization of the ennobled coupons.

Metal samples

We used two types of corrosion coupons: (1) 316L stainless steel and (2) Ti-6Al-4V, each 1.6 cm in diameter. Both materials were cut from larger sheets provided by Metal Samples, Inc. (Munford, AL). Tables 1 and 2 show the composition of these materials, as provided by the vendor. The coupons were polished as described in our previous paper [24] to provide a mirror finish surface sufficiently free of flaws for surface analyses. Then the coupons were sonicated, first in acetone, then in 95% ethanol, each for five minutes, to remove any residual oil based contamination. The coupons were air dried and mounted in polycarbonate holders using a slow hardening epoxy (Buehler Epoxide). Electrical connections were made, to monitor OCP of the coupons, by attaching conductive springs to the back of the coupons inside the holders. Prior to ennoblement experiments, the coupons were left in contact with atmospheric air for 24 h to form a protective surface layer of metal oxides.

TABLE 1
ELEMENTAL COMPOSITION (WT. %) OF 316L STAINLESS STEEL CORROSION COUPONS.

Fe	Cr	Ni	Mo	Mn	Si	P	N	C	S
Balanced	16.19	10.19	2.10	1.71	0.39	0.034	0.03	0.017	0.001

TABLE 2
ELEMENTAL COMPOSITION (WT. %) OF TI-6AL-4V CORROSION COUPONS.

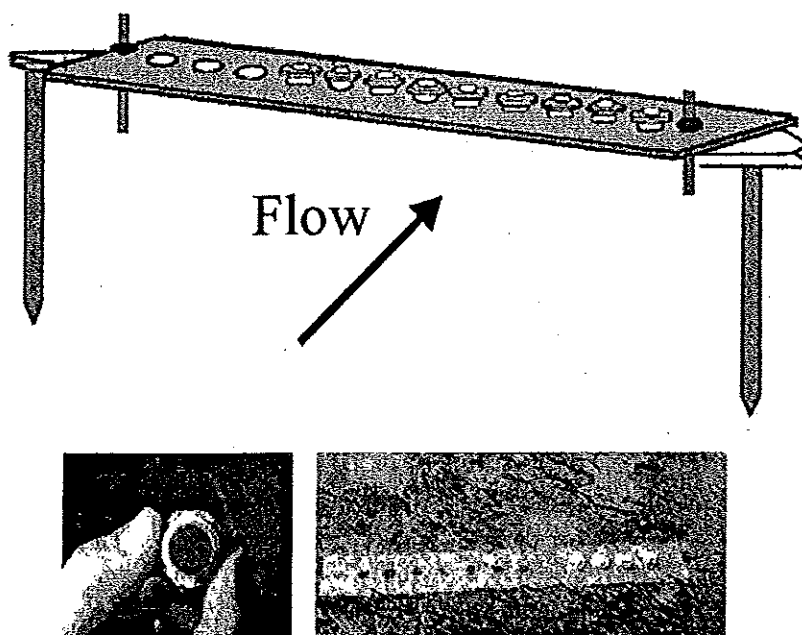| Ti	Al	V	N	C	H	Fe	Mn	O
Balanced	6.0	4.0	0.05	0.1	0.012	0.3	0.01	0.2

FIGURE 1. Coupon holders and frames that were used to expose the stainless steel coupons at the sampling sites. The corrosion coupons were mounted in threaded PVC plugs that were then screwed into

frames constructed of 1/4-inch PVC sheets, 3×12 inches. Coupon holders were fitted with nylon plugs that could be removed to allow access to the backside of the coupon for OCP measurements. Frames were held in place with steel spikes in the stream.

Field studies

For field exposure, we placed a set of 316L stainless steel and Ti-6Al-4V corrosion coupons in the Roskie Creek, a fresh water creek in Bozeman, Montana. This particular site has previously been classified as a clean stream [20]. As shown in Figure 1, the coupons were mounted in a PVC frame and placed face down approximately 10 cm above the sediments. Electrical connections were extended 30 cm above the surface during the measurements and sealed in a waterproof bag between measurements. During 40 days of exposure we checked the set-up and measured OCPs weekly against the saturated calomel reference electrode (SCE). During the time of exposure we verified that the following parameters fluctuated within the boundaries indicated: pH 6.8-7.2, temperature 11-18°C, conductivity 150 μS, Mn^{2+} 60-80 μg/l, Fe^{3+} 300 μg/l, dissolved oxygen 8-9 mg/l.

Electrochemical studies

For all electrochemical studies we used a flat type three-electrode electrochemical cell, with an SCE reference electrode and two high-density graphite counter electrodes. An EG&G Potentiostat/ Galvanostat model 273A was employed, which was interfaced to and controlled by a computer using the 352 SoftCorr III corrosion measurement software by EG&G Princeton Applied Research. To simulate the electrochemistry of stainless steel surfaces covered with biomineralized manganese oxides, we galvanostatically plated manganese dioxide on 316L stainless steel corrosion coupons. The coupons were electroplated in an aqueous electrolyte containing 0.1M Na_2SO_4 and 5mM $MnSO_4$ at pH 6.5, buffered by boric acid and borate. A total charge of 30mC/cm^2 was transferred at a rate of 0.01mA/cm^2, corresponding to a 270 nm thick layer of solid MnO_2.

To identify possible interactions between ferrous ion and manganese oxides on a stainless steel surface, several MnO_2-plated stainless steel coupons were immersed into an aqueous electrolyte containing 0.1M Na_2SO_4, 2.5mM $FeSO_4$, and 1mM $MnSO_4$, buffered by boric acid and borate at pH 6.8. During the 48h immersion, the solution was purged with argon to avoid any possible involvement of oxygen. The coupons were then rinsed with distilled water and prepared for OCP measurements and surface analyses.

To evaluate the effects of biomineralized oxides on material integrity, the coupons before and after the ennoblement were potentiodynamicly polarized at room temperature in 0.01M Na_2SO_4 solution buffered to pH 8.30 using boric acid and borate and air-saturated by vigorous stirring at a constant rate. The coupon, which served as the working electrode, was cleaned with distilled water before mounting it to the electrochemical cell. The exposed area of the coupon was 1 cm^2. The coupon was immersed for 10 minutes before the potentiodynamic measurement was started to equilibrate and to stabilize the metal/solution interface. A cathodic polarization scan was performed potentiodynamicly, at a scan rate of 0.167mV/s. The starting potential was chosen just above the OCP of the working electrode and the scan was terminated at 0.85V$_{SCE}$. Each measurement was repeated at least twice to verify the reproducibility.

ToF-SIMS analysis

ToF-SIMS analyses of the coupons and oxide standards were conducted using a Phi-Evans TRIFT I mass spectrometer [31]. The working principle of this system can be found in advanced texts on surface analytical techniques[31-33] and in our earlier publication [24]. Basically, ToF-SIMS is an imaging mass spectroscopy analysis, which allows obtaining a high-resolution mass spectroscopy and high-resolution chemical maps. The analyses were accomplished by rastering a focused primary ion beam across the surface of interest while collecting secondary ions at each point.

We used a pulsed gallium liquid metal ion gun (LMIG) fired at 25 keV primary energy (corresponding to 22 keV impact energy), with a 10-kHz repetition rate, as the primary ion source. A multi-stop time-to-digital converter (TDC) recorded the time of flight of the ion fragments with a 138-ps precision. The LMIG pulse width was kept <14 ns while the raster size of the beam varied from 80×80 μm^2 to 240×240 μm^2, combination of all of which yielded ~ 1μm spatial resolution while simultaneously detecting ion fragments with ~m/Δm ~2000 mass resolution. In all of the ToF-SIMS acquisitions we stayed within the limit of static SIMS requirements, which means the primary ion dose remained below 10^{13} ions per cm^2. A beam of low-energy (<20 eV) electrons was fired intermittently to prevent charging of the sample. The data acquisition and analysis were done using both DOS and Win-Cadence ToF-SIMS software (Physical Electronics).

To analyze the surface chemistry of electroplated coupons, we rinsed the metal surface carefully with distilled water to clean any soluble salt that may exist. To analyze the surface chemistry of the ennobled coupons, we gently removed the biofilm using acetone, distilled water and a paper tissue. The coupons were then mechanically removed from the holders, air-dried and kept in separate airtight containers for up to 24 h prior to SIMS analysis to ensure dryness. After the SIMS analysis we carefully removed the deposits from each coupon by sanding the surface with 0.05-μm polishing powder and then rinsing with distilled water. The SIMS spectra of each coupon surface were collected again. We used the latter results as controls, reflecting the chemistry of the bare metal surface after ennoblement or electroplating.

Six manganese oxides were used as standards to collect their SIMS reference spectra. We chose MnO_2, MnOOH, Mn_3O_4, and $MnCO_3$ because they are reportedly the predominant species of manganese oxides in natural waters [22]. In addition, we chose MnO and Mn_2O_3 to include other oxidation states of manganese that could be present on the ennobled coupons. Five of the oxides were commercial products from Aldrich Chemical Company, Inc.: MnO (99%), Mn_2O_3 (99%), MnO_2 (99%), Mn_3O_4 (97%) and $MnCO_3$ (99.9+%). The sixth was a natural sample of the mineral manganite (MnOOH) from Wards Natural Science Establishment, Inc. The sample of MnOOH was cut, fractured, and immediately inserted into the analysis chamber in vacuum to minimize surface contamination. From the x-ray powder diffraction patterns we verified that the sixth sample was pure manganite (δ-MnOOH) [33]. We also used four iron oxides, FeO (99.9%, Aldrich), Fe_2O_3 (99.999%, ACROS), Fe_3O_4 (Lab. grade, Fisher), and FeOOH (99.8%, Strem), as standards to collect their SIMS reference spectra. They make up of the spectrum of the possible states of biomineralized iron in the microbial deposits since no iron sulfides were identified.

We prepared the mineral standards for SIMS analysis by gently pressing the powdered compounds into a piece of soft indium foil (Alfa, ESAR), using clean glass slides to ensure that the surface to be analyzed was flat. As a result, the sample spectra included a peak from indium, but this did not interfere with any peaks of importance for this study.
Region-of-interest analysis

Since the microbial deposits were not uniformly distributed on the surface, we needed to eliminate the areas that were not covered by deposits and determine the composition of the deposits only. The raw data acquisition of ToF-SIMS stores a complete mass spectrum for each of the 256×256 pixels uniformly distributed through the area of interest. Retrospective analysis of the raw SIMS data files makes it possible to obtain chemical maps of the specific ion fragments of our choice. To determine the chemical composition of microbial deposits, we extract the SIMS spectra using what is known as "region-of-interest" (ROI) acquisition during a retrospective analysis of "raw" data files [31]. An ROI was defined by using a simple drawing tool to select the areas in a SIMS image from which mass spectra were acquired. This way we minimized the contributions from the bare surface.

RESULTS AND DISCUSSION

Attribution of secondary ion peaks

We made use of the chemical imaging capabilities of ToF-SIMS and studied the surface chemistry of a MnO_2-plated stainless steel coupon by collecting SIMS data from a 180×180 μm^2 area on the surface. Figure 2 shows the distribution of secondary ions: Mn^+, FeH^+, Cr^+, and Fe^+, corresponding to the peaks at approximately 55amu, 57amu, 52amu, and 56amu, respectively.
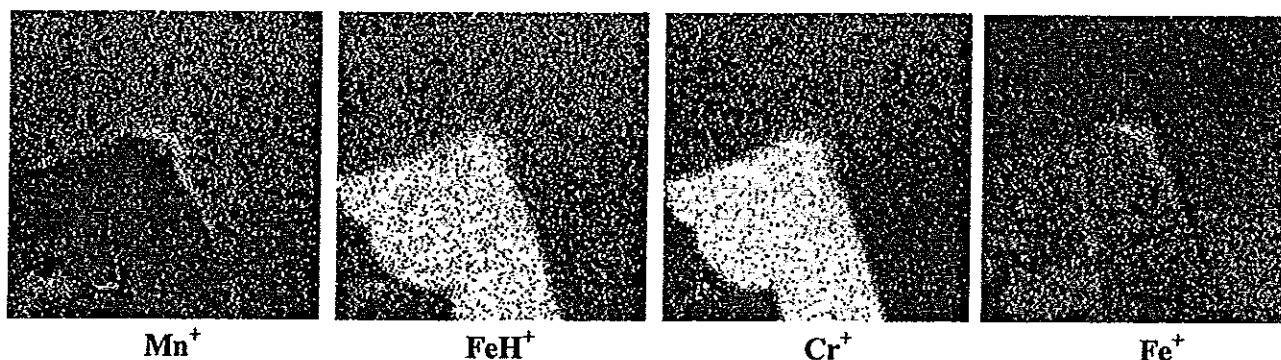

Mn^+ FeH^+ Cr^+ Fe^+

FIGURE 2. ToF-SIMS images showing the distribution of secondary ions: Mn^+, FeH^+, Cr^+, and Fe^+. Data collected from a 180×180 μm^2 area on a 316L stainless steel electroplated with MnO_2. The SIMS peak of Fe^+ was confounded by the presence of MnH^+. The white areas show low concentrations.

For the SIMS images, different colors indicate different intensities of the specific secondary ion. In this paper, we used the black-and-white format, i.e., white color indicates low intensity whereas black color indicates high intensity, which also applies to Figure 3. In the Mn^+ map, the strong signals in the black regions indicate the presence of MnO_2 layer while the Mn^+ signals in other regions come from the stainless steel itself. In the regions covered by MnO_2, both FeH^+ and Cr^+ are depleted while Fe^+ appears to be still present, but as explained below this mass (56 amu) is mostly due to MnH^+ rather than Fe^+. The identification of the SIMS peaks of interest are as follows: Mn^+(~55amu), FeH^+(~57amu), and Cr^+(~52amu). The Fe^+ map suggests that the peak at approximately 56amu is actually the result of the presence of both Fe^+ and MnH^+. Therefore, in the regions covered by MnO_2, the signals are actually MnH^+, not Fe^+. For this reason we used FeH^+, instead of Fe^+, to map the distribution of iron minerals on the metal surface. For cases where both Mn and Fe contributions are present simultaneously we developed a multivariable regression analysis technique as described in Appendix I to separate the Fe^+ and MnH^+ components of a peak at 56 amu.

Chemical imaging of the field-ennobled coupons

With the imaging capabilities of ToF-SIMS, we generated chemical maps of spatial distribution of the secondary ions of interest on the surface of a Ti-6Al-4V coupon ennobled to +400mV$_{SCE}$ in the Roskie creek. The coupon was cleaned carefully with distilled water and paper tissue such that part of the biofilm and most of the biominerals were kept on the surface.

Figure 3 shows the distributions of secondary ions, Ti^+, Mn^+, and FeH^+, on the Ti-6Al-4V coupon, which were generated from the same 180×180 μm^2 area. FeH^+, instead of Fe^+, was used to map the distribution of iron oxides, because the latter cannot be separated from the signals of MnH^+ in the SIMS spectra without numerical analysis. In the Ti^+ map, the depleted signals in the white regions indicate that they are covered by the residual biofilm, while the strong signals in the black regions indicate the absence of biofilm. In the regions not covered by biofilm, both Mn^+ and FeH^+ are enriched, which can be attributed to the presence of Mn-rich microbial deposits and Fe in the metal substratum. In the regions covered by biofilm, however, Mn^+ is significantly enriched and FeH^+ is also present while Ti^+ is depleted. This is an expected result because Ti^+ comes from the metal substratum only while the Mn^+ and FeH^+ signals are coming from the microbial deposits. Therefore, we hypothesized that there was biomineralized manganese as well as iron in the biofilm and microbial deposits, which was confirmed by the quantitative ROI analyses. The semi-quantitative analysis in terms of areas under the peaks of the SIMS spectra further suggested that the amount of biomineralized manganese is higher than that of iron minerals in the biofilm.
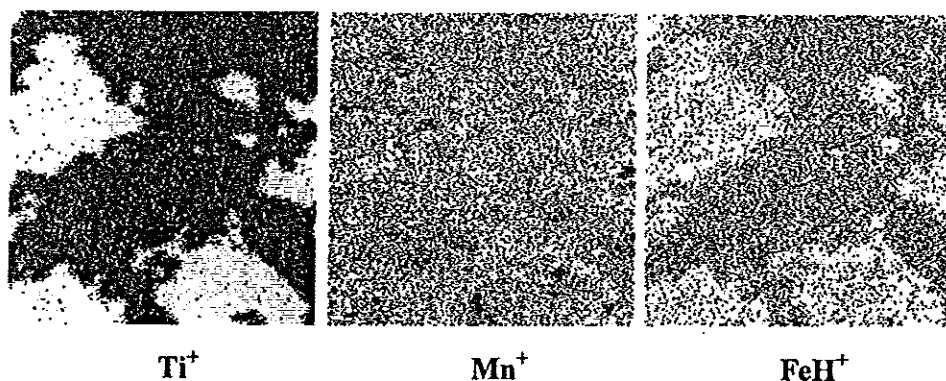

| Ti^+ | Mn^+ | FeH^+ |

FIGURE 3. ToF-SIMS images showing the distribution of secondary ions: Ti^+, Mn^+, and FeH^+. Data collected from a 180×180 μm^2 area on a Ti-6Al-4V coupon ennobled to +400mV$_{SCE}$ in the Roskie creek. The white areas show low concentrations.

Chemical composition of microbial deposits

As demonstrated by our previous ToF-SIMS studies of microbial deposits on metal coupons ennobled under well-defined laboratory conditions [24], there is a clear relationship between the ratios of certain signal intensities in the SIMS spectra and the oxidation state of the oxides. The relative intensities of the secondary ions can thus be used to identify the oxidation state of each oxide. This technique can be applied to identify unknown manganese oxides and iron oxides deposited on the metal surfaces. For a mixture of minerals, it is also possible to determine the mixing fraction of each oxide by making use of the SIMS data of well-defined standards and by using the lever rule: $R=xR_1+(1-x)R_2$, where R_1 and R_2 are standard ratios, R is the measured ratio and the x is the mixing fraction of oxide 1.

To identify various oxides and to quantify their observed differences, we used two groups of ratios of signal intensities as indicators: MnH^+/Mn^+ and FeH^+/Fe^+ from the positive ion spectra. To achieve statistical reliability, we collected the SIMS spectra from 6~7 different areas on each sample (manganese/iron standards or metal coupons), and then calculated the mean value and subsequently the standard deviation of the ratios using the procedure we developed as explained in Appendix I. Ratios from the negative ion spectra, such as $MnOH^-/MnO^-$ and $FeOH^-/FeO^-$, are less accurate mostly likely due to low signal levels and to the interference of organics left on the metal surface and thus were only used as additional information for confirmation.

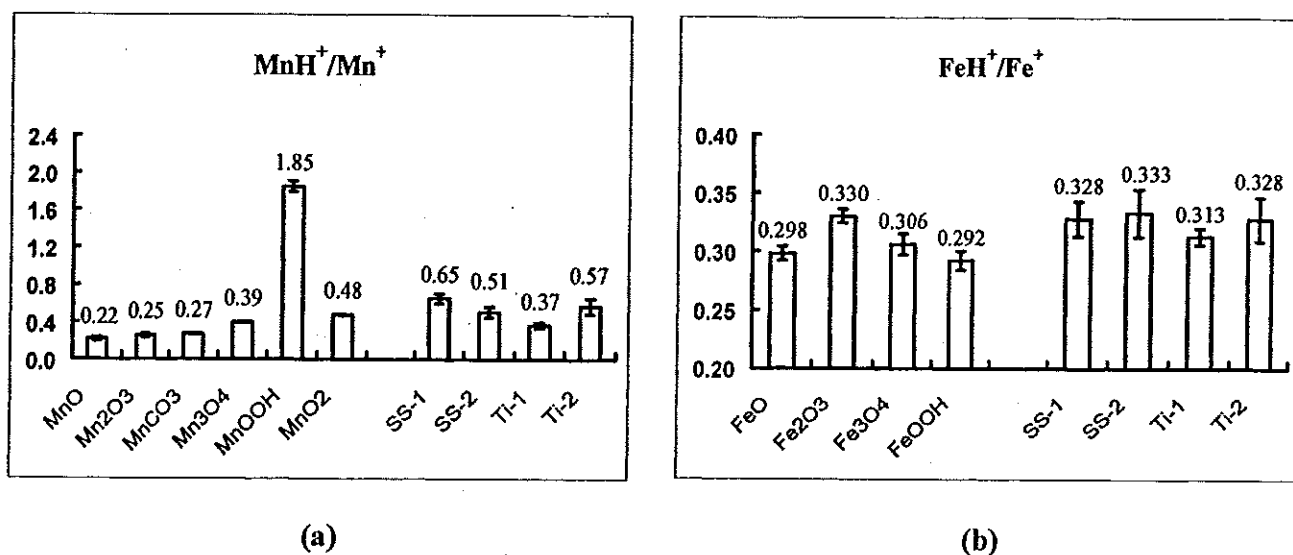(a)   (b)

FIGURE 4. Intensity ratios of secondary ions in the SIMS spectra as a function of oxide standards and unknown minerals on various ennobled coupons: (a) MnH^+/Mn^+ and (b) FeH^+/Fe^+. The ratios, along with mass spectroscopy and chemical map information provided by the SIMS analysis, suggest that the biomineralized manganese on fully ennobled 316L stainless steel (*SS-1*, *SS-2*: $+365mV_{SCE}$) and Ti-4Al-6V (*Ti-2*: $+400mV_{SCE}$) surfaces is a mixture of MnOOH and Mn_3O_4, whereas the biomineralized iron is mostly Fe_2O_3. For partially ennobled Ti-4Al-6V (*Ti-1*: $+350V_{SCE}$) surface, the biomineralized manganese is a mixture of Mn_3O_4 and Mn_2O_3, and the biomineralized iron is Fe_3O_4, mixed with a certain amount of Fe_2O_3.

In the SIMS analysis of the ennobled coupons the signals of Mn^+ and Fe^++MnH^+ from the metal substratum contribute to those from the microbial deposits that we aim to identify. This contribution is eliminated by collecting SIMS spectra both from the ennobled coupon and from the metal surface with microbial deposits removed. As described below, the contribution from the bare metal substratum is subtracted off and the difference is used as the signal from the microbial deposits alone. In order to determine the substrate contribution for 316L stainless steel, we used Cr^+ as the internal intensity reference peak for normalization purposes, assuming it is not influenced by the microbial activities. We subtracted the normalized substratum contributions from the SIMS counts to determine the signals due to the biominerals. Similarly, for Ti-6Al-4V Ti^+ was used as the internal reference peak for normalization. In Appendix I we give an example of the typical procedure for performing background subtraction and subsequent multivariable regression analysis technique to separate the MnH^+ and Fe^+ components of the peak at 56 amu to determine the true MnH^+/Mn^+ and FeH^+/Fe^+ ratios due to biominerals. The results of such analysis are described below. Figure 4a and 4b show the appropriate

MnH^+/Mn^+ and FeH^+/Fe^+ intensity ratios, respectively, as a function of six manganese oxide standards (Fig. 4a), and four iron oxide standards (Fig. 4b), and as a function of samples: a partially ennobled Ti-6Al-4V (*Ti-1*: +350mV$_{SCE}$), a fully ennobled Ti-4Al-6V (*Ti-2*: +400mV$_{SCE}$), two ennobled 316L stainless steel (*SS-1, SS-2*: +365mV$_{SCE}$) coupons. The standard deviation of the intensity ratios relative to the mean values varies from 7% to 18%. The high standard deviations may be due to variations in the chemical composition of microbial deposits at microscopic scale and due to variations in the substrate matrix from which the secondary ions are generated. For example, our previous work using XPS analysis[22] indicated that there were two or more manganese minerals with different oxidation states within the microbial deposits in natural waters. In addition, presence of organics may affect the secondary ion generation associated with the inorganic species. XPS depth profiling of the microbial mineral deposits by other members of our group confirmed the presence of organic species in these films. In spite of such uncertainties, the ToF-SIMS fragmentation patterns of manganese and iron standards are of great diagnostic value in determining the identification of inorganic microbial deposits on the ennobled or partially ennobled surfaces with reasonable confidence and accuracy.

The intensity ratio of MnH^+/Mn^+ in the SIMS data can be used to identify the oxidation state of biomineralized manganese. As shown in Figure 4a, the mean values of MnH^+/Mn^+ in the SIMS spectra of biominerals on *SS-1, SS-2, and Ti-2* (0.65, 0.51, 0.57) appears to lie between that of Mn_3O_4 (0.39) and $MnOOH$ (1.85), as well as between MnO_2 (0.48) and $MnOOH$ (1.85). Some individual observations on a number of spots revealed that MnH^+/Mn^+ ratios are less than 0.400 with no manganese carbonate identified in the SIMS spectra, therefore, the presence of Mn_3O_4 is expected. Based on the comparison of the two Ti-6Al-4V coupons, where the partially ennobled coupon has lower mean value of MnH^+/Mn^+ (0.37) than the fully ennobled one (0.57), the possibility of a mixture of MnO_2 and $MnOOH$ was ruled out. We hypothesized that the biomineralized manganese on ennobled coupons is a mixture of Mn_3O_4 and $MnOOH$, perhaps mixed with very small amount of MnO_2. The mean value of MnH^+/Mn^+ in the SIMS spectra of biominerals on *Ti-1* (0.37) appears to lie between that of Mn_2O_3 (0.25) and Mn_3O_4 (0.39). Since no manganese carbonate was identified in the SIMS spectra, we concluded that the biomineralized deposits on the partially ennobled metal surface consists of Mn_3O_4 and Mn_2O_3. As a result of MOB activities in natural waters, the manganese is expected to evolve from Mn^{2+} to Mn_3O_4 and Mn_2O_3, and then Mn_2O_3 transforms to $MnOOH$, and the OCP increases accordingly. It is interesting to note that the mechanism described above of manganese biomineralization in natural waters is somewhat different from that is observed in well-defined laboratory conditions. In the latter the manganese biomineralization by *Leptothrix Discophora SP-6* occurs in two steps [24]: first, Mn^{2+} is oxidized to $MnOOH$; then $MnOOH$ is further oxidized to MnO_2. Both mechanisms, however, are at least partly responsible for the observed OCP increase during the ennoblement process. The difference in manganese biomineralization can be explained by the presence of various types of microorganisms in natural waters including bacteria, yeast, and fungi. In addition, we observed that the extracellular polymer substances (EPS) in natural waters were much more adherent to the metal surface, which implicates that EPS played an important role in the ennoblement process in natural waters.

The intensity ratio of FeH^+/Fe^+ in the SIMS data, too, can be used to identify the oxidation state of biomineralized iron. As shown in Figure 4b, the mean value of FeH^+/Fe^+ in the SIMS spectra of microbial deposits on *SS-1, SS-2, and Ti-2* (0.33) is close to that of Fe_2O_3 (0.33). Therefore, we hypothesized that the biomineralized iron on ennobled coupons is mainly Fe_2O_3. The mean value of FeH^+/Fe^+ in the SIMS spectra of microbial deposits on *Ti-1* (0.313) is between that of Fe_3O_4 (0.306) and Fe_2O_3 (0.330). Given the uncertainties in these ratios the two values are indistinguishable. Based on the thermodynamics, we hypothesized that the biomineralized iron on partially ennobled metal surfaces consists of Fe_3O_4 and Fe_2O_3. As the OCP increases, the iron evolves from lower oxidation state to higher

ones, i.e., from Fe^{2+} to Fe_3O_4, then to Fe_2O_3, as a result of IOB activities or simply because of the OCP increase caused by MOB activities.

The simulation of coexistence of manganese and iron oxides

Experiments were conducted by immersing MnO_2-plated stainless steel coupons into the solution of divalent iron (2.5mM FeSO$_4$). It was noted that the immersion did not cause any apparent change in the OCP of the metal samples, which stayed at around +360mV$_{SCE}$ in a solution of pH 7.2 and Mn^{2+} concentration of 1×10^{-6} M. We analyzed the surface chemistry before and after the immersion using ToF-SIMS. The mean value of MnH^+/Mn^+ of the surface deposits on the SS coupons before and after immersion was 0.43 and 1.12, respectively, which indicates a plated layer of MnO_2 (0.48) before immersion and a mixture of MnO_2 (0.48) and MnOOH (1.85) after immersion. The mean value of FeH^+/Fe^+ of the surface deposits on the SS coupons after immersion (0.35) indicates the formation of Fe_2O_3 (0.33). We concluded that the manganese dioxide deposited on stainless steel coupons was reduced to MnOOH by oxidizing the divalent iron to Fe_2O_3, indicating that ferrous ion is a reductant of Mn(IV) oxides. In addition, the formed Fe_2O_3 seemed to be a stable product on the ennobled coupon and did not decrease the OCP of the coupon. Consequently we hypothesized that manganese oxides maintained the OCP of the metal coupons and the presence of iron oxides within the microbial deposits had little effect on the OCP of field-ennobled coupons.

Impact of biomineralization on the cathodic polarization curves

As a measure of material performance, the typical potentiodynamic polarization curves were obtained for non-ennobled, partially ennobled, and fully ennobled stainless steel coupons, as shown in Figure 5. The partially and fully ennobled stainless steel coupons had biofilm coverage of approximately 100% and 95%, respectively.

Both partially and fully ennobled coupons shifted corrosion potentials several hundred millivolts in the noble direction. Polarization curves also show a corresponding increase in cathodic current density at modest overpotentials, for example, a 70mV cathodic overpotential on non-ennobled coupons generates a current density of approximately 10^{-8} A/cm^2 while it generates more than two orders of magnitude current density ($\sim 10^{-6}$ A/cm^2) on fully ennobled coupons. The results are in accordance with our previous publications [19,20], which suggested that the increase in OCP and cathodic current density is most likely due to the presence of microbially deposited oxides on the stainless steel surface and indicates the decrease of corrosion resistance of the material. As shown in Figure 5, the polarization curves for partially and fully ennobled stainless steel coupons show similar cathodic current behaviors during the cathodic polarization scan, whereas the fully ennobled coupon has a higher corrosion potential (+0.330mV$_{SCE}$ vs. +0.220mV$_{SCE}$). The results suggest that biomineralized manganese and iron oxides on the 316L stainless steel surfaces, regardless of their different oxidation states as indicated by our SIMS analyses, impact the material performance in a similar manner. Based on our potentiodynamic polarization measurements, we concluded that the biomineralized manganese and iron oxides deposited on the metal surface exhibits lower corrosion resistance and thus exposes higher risk of localized corrosion. The possible correlation between the distribution of biomineralized manganese and iron oxides and that of localized corrosion is the subject of our ongoing research.
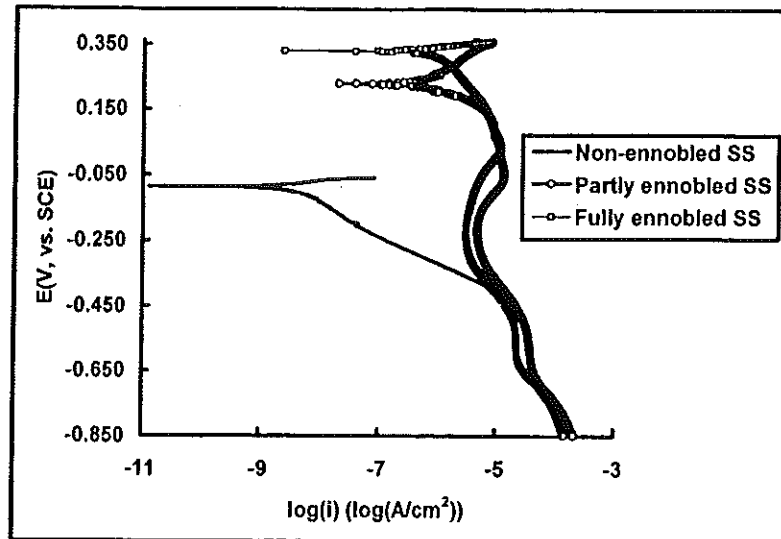
FIGURE 5. Potentiodynamic polarization curves (obtained in 0.01M Na_2SO_4 test solution, pH 8.30, scan rate: 0.167mV/s) typical for stainless steel coupons ennobled in the field to different degrees. The partially and fully ennobled stainless steel coupons show a similar Tafel slope and similar cathodic current densities at modest overpotentials, even though the fully ennobled coupon has a higher corrosion potential. The curve corresponding to non-ennobled SS (full line) is also shown for comparison.

CONCLUSIONS

1) With micro-chemical imaging capabilities and high detection sensitivity, a surface analysis technique based on ToF-SIMS was developed to identify the oxidation states and distribution of biominerals on 316L SS and Ti-6Al-4V corrosion coupons ennobled in natural waters. ToF-SIMS spectra of the microbial deposits compared to spectra of different manganese and iron mineral standards indicated that the deposits are a mixture of Fe_3O_4, Fe_2O_3, Mn_3O_4, and Mn_2O_3 on partially ennobled coupons, while a mixture of Fe_2O_3, Mn_3O_4, and $MnOOH$ on fully ennobled coupons.

2) The biomineralized manganese and iron oxides on 316L stainless steel were responsible for the elevated OCP and corresponding increase in cathodic current density. Regardless of their oxidation states, the biomineralized oxides affected the material performance in a similar manner.

ACKNOWLEDGEMENT

Table 3 gives an example of determining the counts due to microbial deposits for seven different regions on the surface of an ennobled Ti-6Al-4V coupon, *Ti-2* (ennobled to +400mV$_{SCE}$). Columns 1 ~ 4 show the raw counts (areas under the peaks), I_T, of Mn^+, MnH^++Fe^+, FeH^+, and Ti^+. Columns 5 ~ 7 show the subtracted counts, I, due to biominerals. Columns 8 and 9 show the individual components αI_1 (MnH^+) and βI_2 (Fe^+) of MnH^++Fe^+ (Column 6) determined by multiple regression. The sum of Columns 8 and 9 is roughly equal to Column 6 (Formula 2). The last row (labeled as ρ) shows the intensity ratios of Mn^+, MnH^++Fe^+, and FeH^+ to Ti^+, respectively, for the bare metal surface obtained after removing the biominerals from the ennobled coupon by means of polishing the surface very lightly. Also shown in this row are the parameters α and β, the ratios MnH^+/Mn^+ and FeH^+/Fe^+ and their standard deviations.

Background subtraction

Equation 1 below is the relation used for subtracting background contributions:

$$I = I_T - \rho I_R \qquad (1)$$

In this formula I represents the subtracted counts corresponding to any of the Mn^+, MnH^++Fe^+, or FeH^+, attributed to the microbial deposits alone (Table 3, columns 5-7), I_T represents any of the total Mn^+, MnH^++Fe^+, or FeH^+ counts from the ennobled coupon, including those from the substratum surface and from the deposits (Table 3, columns 1-3); I_R is the counts of the reference peak from the ennobled coupon (column 4), which is chosen to be Cr^+ or Ti^+ depending on whether a 316L stainless steel or Ti-6Al-4V (as in example) is used as substrate; ρ is the mean value of the intensity ratios between any of the Mn^+, MnH^++Fe^+, or FeH^+ of the *bare metal surface* and the reference peak, in our case Ti^+. These ratios are listed in the last row of Table 3. Next we give the procedure to determine the individual contributions from MnH^+ ions and Fe^+ ions to the MnH^++Fe^+ intensity (Column 6 of Table 3).

Determination of MnH^+ and Fe^+ using multivariable regression analysis

Column 6 of Table 3 gives the background-subtracted peak intensity corresponding to MnH^++Fe^+ which contains contributions from both the MnH^+ and Fe^+ ions. The basic approach here is to assume that the net MnH^++Fe^+ counts, I, from a given region as shown on Column 6 can be expressed as a linear combination of the net Mn^+ counts, I_1, (Column 5) and the net FeH^+ counts, I_2 (Column 7). This is supported by the fact that the FeH^+ peak does not receive much contribution from the manganese due to low MnH_2^+ yield. Experiments showed that this contribution was only ~ 2% of Mn^+ intensity and this value was subtracted off from the raw FeH^+ intensity (Column 3). On the other hand the MnH^+ comprises a substantial fraction of Mn^+ yield and cannot be differentiated from Fe^+. The Equation 2 below is, in effect, a matrix equation correlating Column 6 to Column 5 and 7 using two parameters, α and β via

$$I = \alpha I_1 + \beta I_2 \qquad (2)$$

where the coefficients α and β were determined applying the multivariable linear regression technique [34] using the data listed in Colunms 5 and 7. Since there were two unknown parameters, α and β, we collected data from seven different regions on the surface of the same sample, *Ti-2*. The results of multiple regression analysis readily yield α=0.570±0.086 and β=3.053±0.055 (bottom row).

Using the α and β and the Equation 2 above we calculated the predicted contributions αI_1 (MnH$^+$) and βI_2 (Fe$^+$) to the peak around 56amu and the results are given in Columns 8 and 9, respectively. The mean values and the standard deviations of the ratios MnH$^+$/Mn$^+$ and FeH$^+$/Fe$^+$ can now readily be determined to be 0.570±0.086 and 0.328±0.018, respectively (bottom row). Since the standard deviations are within reasonable range, the ratios MnH$^+$/Mn$^+$ and FeH$^+$/Fe$^+$ were used to identify the oxidation state of biomineralized manganese and iron as discussed in the text.

TABLE 3

AN EXAMPLE OF APPLYING EQUATIONS 1 AND 2 TO DETERMINE THE COUNTS DUE TO MICROBIAL DEPOSITS AND THE TRUE RATIOS OF MNH$^+$/MN$^+$ AND FEH$^+$/FE$^+$.

Region	(1) Mn$^+$	(2) (MnH$^+$ +Fe$^+$)*	(3) FeH$^+$	(4) Ti$^+$	(5) Mn$^+$	(6) (MnH$^+$ +Fe$^+$)*	(7) FeH$^+$**	(8) MnH$^+$	(9) Fe$^+$
1	1731	4189	1072	26358	1656	3930	937	1069	2986
2	35623	97481	28317	515981	34157	92417	25635	14156	72947
3	47443	122043	31758	732775	45361	114851	28012	29334	88995
4	14344	21964	4428	746	14342	21957	4138	9324	13782
5	6207	8921	1803	307	6206	8918	1678	3795	5380
6	13549	20622	4354	774	13547	20614	4080	8158	12892
7	3331	4641	1008	171	3331	4639	941	1766	2740
ρ	2.84×10^{-3}	9.81×10^{-3}	3.87×10^{-3}	1	α=0.570±0.086 β=3.053±0.055			MnH$^+$/Mn$^+$=0.570 FeH$^+$/Fe$^+$= 0.328	

REFERENCES

1. W. H. Dickinson, Z. Lewandowski, Biofouling 10 (1996): p. 79.
2. W. A. Hamilton, Microbially influenced corrosion in the context of metal microbe interactions, in: L. V. Evans (Ed.), Biofilms: Recent advances in their study and control, Harwood Academic Publishers, 2000, pp. 419-434.
3. Z. Lewandowski, W. Dickinson, W. Lee, Wat. Sci. Tech. 30, 1 (1997): p. 295.
4. B. J. Little, P. A. Wagner, Z. Lewandowski, Proceedings of Corrosion 1998, (Houston, TX: NACE, 1998), Paper No. 294.
5. P. Linhardt, Materials Science Forum 289-292 (1998): p.1267.
6. H. Volkland, H. Harms, B. Muller, G. Repphun, O. Wanner, A. J. B. Zehnder, Appl. Env. Microb. 66, 10 (2000): p. 4389.
7. I. G. Chamritski, G. R. Burns, B. J. Webster, N. J. Laycock, Proceedings of Corrosion 2001, (Houston, TX: NACE, 2001), Paper No. 01254.
8. S. D. Strauss, Power, 135, (1991): p. 50
9. A. Mollica, "The Influence of the Microbiological Film on Stainless Steels in Natural Seawater", 4th International Congress on Marine Corrosion and Fouling, pp.351-365 (Antibes, France, 1976).
10. V. Scotto, R. DiCintio, G. Marcenaro, Corr. Sci. 25, 3 (1985): p.185.

---

* The two peaks cannot be resolved without numerical analysis.
** The counts due to Mn H$_2^+$ were subtracted, the intensity of which was determined to be about 2% of Mn$^+$.

11. R. Johnsen, E. Bardal, Corrosion 41, 5 (1985): p. 296.
12. S. C. Dexter, G. Y. Gao, Corrosion 44, 10 (1988): p.717.
13. S. Motoda, Y. Suzuki, T. Shinohara, Corr. Sci. 31 (1990): p.515.
14. P. Chandrasekaran, S. C. Dexter, Proceedings of Corrosion 1993, (Houston, TX: NACE, 1993), Paper No. 493.
15. M. Eashwar, S. Maruthamuthu, Biofouling 8 (1995): p.203.
16. W. H. Dickinson, F. Caccavo Jr, Z. Lewandowski, Corrosion Sci. 38, 8 (1996): p.1407.
17. P. Linhardt, Failure of chromium-nickel steel in a hydroelectric power plant by manganese-oxidizing bacteria, in: E. Heitz, H-C, Flemming, W. Sand (Eds.), Microbially influenced corrosion of materials, Springer Berlin Heidelberg, 1996, pp. 221-230.
18. P. Linhardt, Werkstoffe und Korrosion 45 (1994): p.79.
19. W. Dickinson, Z. Lewandowski, Proceedings of Corrosion 1995, (Houston, TX: NACE, 1993), Paper No. 223.
20. W. Dickinson, Z. Lewandowski, R. D. Geer, Corrosion 52, 12 (1996): p. 910.
21. B. H. Olesen, R. Avci, Z. Lewandowski, Proceedings of Corrosion 1998, (Houston, TX: NACE, 1998), Paper No. 275.
22. B. H. Olesen, R. Avci, Z. Lewandowski, Corr. Sci. 42, 2 (2000): p. 211.
23. W. H. Dickinson, F. Caccavo Jr, B. H. Olesen, Z. Lewandowski, Appl. Env. Microb. 63, 7 (1997): p. 2502.
24. X. Shi, R. Avci, Z. Lewandowski, Corr. Sci., (2001), in publication.
25. A. Gounot, FEMS Microbiology Reviews, 14 (1994): p.339.
26. K. H. Nealson, B. M. Tebo, R. A. Rosson, Advances in Applied Microbiology, 33 (1988): p.279.
27. R. Schweisfurth, G. Gattow, Z. Allg. Mikrobiol. 56 (1966): p.303.
28. G. Kobrin, Materials Performance, July Issue, (1976): p.38
29. N. M. Reed, J. C. Vickerman, Static SIMS – Surface Analysis of Inorganic Materials, in: D. Briggs, M. P. Seah (Eds.), Practical Surface Analysis, 2nd Edition, Vol.2 – Ion and Neutral Spectroscopy, John Wiley & Sons, 1996, pp.303-366.
30. S. S. Cristy, Secondary Ion Mass Spectrometry, in: C. M. Barshick, D. C. Duckworth, D. H. Smith (Eds.), Inorganic Mass Spectrometry: Fundamentals and Applications, Marcel Dekker, New York, 2000, pp.159-221.
31. O. Gebhardt, Fresenius, J. Anal. Chem. 365 (1999): p.117.
32. D. Briggs, A. Brown, J. C. Vickerman, Handbook of Static Secondary Ion Mass Spectrometry, John Wiley & Sons, 1990.
33. H. W. Nesbitt, D. Banerjee, Amer. Mineral. 83 (1998): p.305.
34. C. R. Hicks, K. V. Turner, Fundamental Concepts in the Design of Experiments, 5th Edition, Oxford University Press, 1999, pp424-430.